tion, a single universal administered activity schedule is suggested that would lead to good uniformity of effective dose over the pediatric range (COV ≤ 10%) for the radiopharmaceuticals examined. This is provisional on there being no significant age-dependent properties that invalidate the application of a common biokinetic model for dose calculation of a given radiopharmaceutical.

ACKNOWLEDGMENTS

This study was based on work supported in part by the Commission of European Communities, Nuclear Fission Safety Programme (contract F13P-CT920052).

REFERENCES

1. Evans K, Lythgoe MF, Anderson PJ, Smith T, Gordon I. Biokinetic behavior of technetium-99m-DMSA in children. *J Nucl Med* 1996;37:1331–1335.
2. Smith T, Evans K, Lythgoe MF, Anderson PJ, Gordon I. Radiation dosimetry of technetium-99m-DMSA in children. *J Nucl Med* 1996;37:1336–1342.
3. Smith T, Evans K, Lythgoe MF, Anderson PJ, Gordon I. Technetium-99m-DMSA in children: biodistribution, dosimetry, radiopharmaceutical schedule and age dependency. In: *Proceedings of the sixth International Radiopharmaceutical Dosimetry Symposium*. Gatlinburg, TN: Oak Ridge Associated Universities; 1996: in press.
4. Cristy M, Eckerman K. Specific absorbed fractions of energy at various ages from internal photon sources. ORNL/TM-8381. Oak Ridge TN: Oak Ridge National Laboratory; 1987.
5. International Commission on Radiological Protection. *Radiation dose to patients from radiopharmaceuticals*. ICRP Publication 53. Oxford: Pergamon Press; 1987:18.
6. International Commission on Radiological Protection. *Radiological protection in biomedical research*. ICRP Publication 62. Oxford: Pergamon Press; 1991:22.
7. Snyder WS, Ford MR, Warner GG, Watson SB. "S", absorbed dose per unit cumulated activity for selected radionuclides and organs. *MIRD pamphlet no. 11*. New York: Society of Nuclear Medicine; 1975.
8. Stabin M. MIRDOSE: personal computer software for internal dose assessment in nuclear medicine. *J Nucl Med* 1996;37:538–546.
9. Cloutier R, Smith S, Watson EE, Snyder W, Warner G. Dose to the fetus from radionuclides in the bladder. *Health Phys* 1973;25:147–161.
10. International Commission on Radiological Protection. *Recommendations of the ICRP*. ICRP Publication 60. Oxford: Pergamon Press; 1990:21.
11. International Commission on Radiological Protection. *Annual limits on intake of radionuclides by workers based on the 1990 recommendations*. ICRP Publication 61. Oxford: Pergamon Press; 1990:21.
12. International Commission on Radiological Protection. *Age-dependent doses to members of the public from intake of radionuclides: part 2*. ICRP Publication 67. Oxford: Pergamon Press; 1993:23:3–4.
13. Pediatric Task Group of the European Association of Nuclear Medicine. A radiopharmaceutical schedule for imaging in pediatrics. *Eur J Nucl Med* 1990;17:127–129.
14. Webster EW, Alpert NM, Brownell GL. Radiation doses in pediatric nuclear medicine and diagnostic x-ray procedures. In: James AE, Wagner HN, Cooke RE, eds. *Pediatric nuclear medicine*. Philadelphia: WB Saunders; 1974:34–58.

Optimization of the Scintigraphic Segmental Anatomy of the Lungs

John S. Magnussen, Peter Chicco, Amanda W. Palmer, Douglas W. Mackey, Michael Magee, I. Provan C. Murray, George Bautovich, Kevin Allman, Geoffrey Storey and Hans Van der Wall

Department of Nuclear Medicine, Concord Hospital; Graduate School of Biomedical Engineering, University of New South Wales; Department of Radiology, St. George Hospital; Nuclear Diagnostics; and Department of Nuclear Medicine, Royal Prince Alfred Hospital, Sydney, New South Wales, Australia

Accurate and reproducible reporting of lung scintigraphy is predicated on a sound knowledge of the segmental anatomy of the lungs. A limited amount of hard data exists about the true segmental anatomy of the lungs. A virtual model of human lungs was created using a CT-based dataset and a Monte Carlo simulation technique to examine the optimal projections for the visualization of each segment in the lungs. **Methods:** Segmental anatomy of the lungs was modeled using CT, cadaveric lungs and standard anatomical texts. The emission, scatter and attenuation of photons was modeled within these virtual lungs and the surrounding tissues. Single segmental lesions were created in eight projections and submitted for blinded reporting to four experienced nuclear medicine physicians to obtain the best views for each segment. **Results:** The anterior and posterior oblique projections yielded the best views for 10 of 18 segments, with the laterals contributing four views, the anterior contributing two views and the posterior contributing one view. The majority of basal segments (six of nine) were best seen in the anterior and posterior oblique projections. **Conclusion:** This model overcomes the major problems associated with experimentation in the normal human and has the potential to provide answers to the major problems of scatter, attenuation and "shine-through" in lung scintigraphy.

Key Words: pulmonary embolism; lung scintigraphy; segmental anatomy; Monte Carlo simulation

J Nucl Med 1997; 38:1987–1991

Virtually all endeavors to investigate the scintigraphic diagnosis of pulmonary embolism, such as the PIOPED (*1,2*) trial, are predicated on the recognition of the segmental anatomy of the lungs. Although this area has been investigated in several early papers, the efforts have been on the basis of phantoms of the lobar anatomy of the lungs (*3,4*), or arbitrary assignments have been made on the basis of the concave or triangular defects at the periphery of the lung (*5*). More recently, the issue has been investigated in the normal human lung (*6*) using scintigraphic techniques. This first prospective attempt to define the scintigraphic segmental anatomy of the lung suffered, however, from the inherent limitations of radiation exposure to normal volunteers and the acquisition of limited projections.

Much of an instructive nature has been written from a "post hoc" point of view, that is, typical segmental defects are recognized after the diagnosis has been made (*7*). Given the paucity of hard data and implicit restrictions in any prospective human studies, we sought to define a model of the segmental anatomy of the lungs in terms of the best available data from published anatomic studies, CT of the major lobar fissures and injection of the segmental bronchi of cadaveric lungs (*8*). A Monte Carlo simulation package was used to generate photons in these "virtual" lungs, allowing the creation and manipulation of segmental defects. To determine the optimal views for the various segments in the experimental model, it was assumed that the "standard" lung scan contains eight projections.

MATERIALS AND METHODS

The original phantom (*9*) was based on CT data from a supine man of a height of 178 cm and weighing 70 kg who was chosen for

Received Sep. 4, 1996; revision accepted Feb. 26, 1997.

For correspondence or reprints contact: John S. Magnussen, MB, BS, FRSM, Department of Nuclear Medicine, Concord Hospital, Hospital Road, Concord, New South Wales, 2139, Australia.

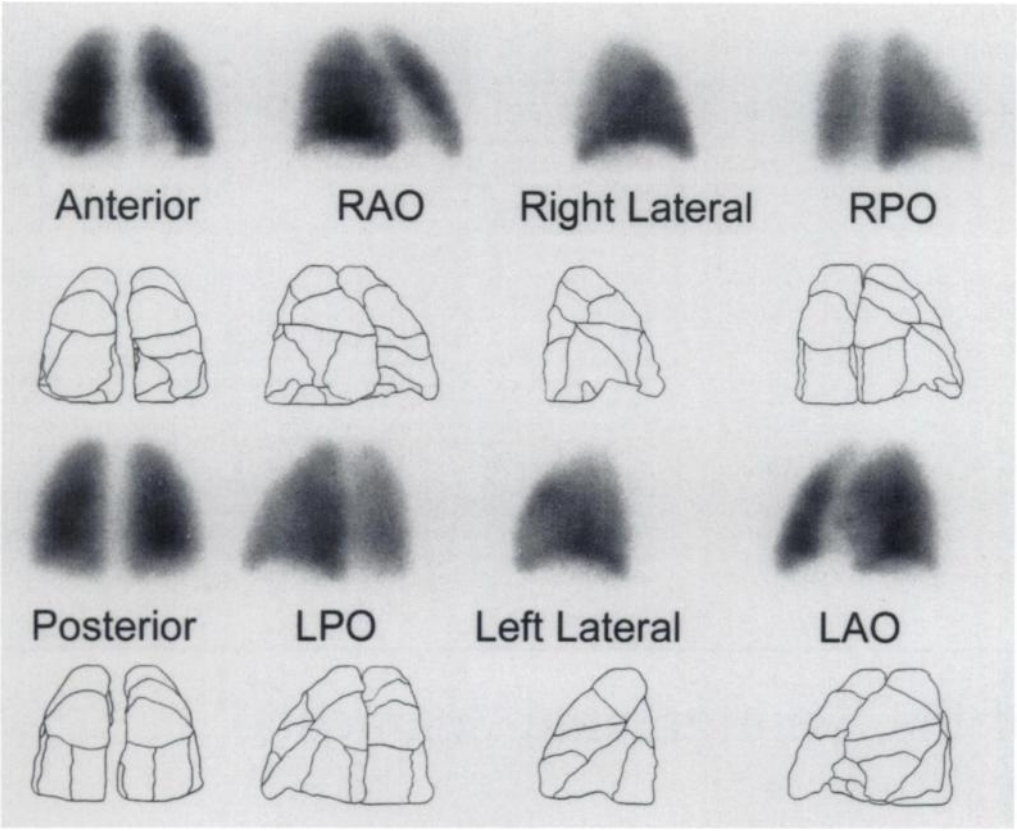

FIGURE 1. Eight views of the Monte Carlo simulated study are shown (upper rows), with the corresponding outlines of the segmented CT phantom (lower rows). RAO, right anterior oblique; RPO, right posterior oblique; LAO, left anterior oblique; LPO, left posterior oblique.

his similarity to the dosimetry standard mathematical phantom (*10*).

The lung tissue in the phantom was segmented in two phases. An experienced radiologist, using patient CT data that showed the interlobar fissures, marked the lobes as a guide to the segments. The segmental bronchi of human cadaveric lungs were injected with color-coded dyes. These were finely sectioned and digitized (*8*). The lobar and segmental boundaries were transferred to the phantom dataset with reference to anatomical texts (*11–13*).

The Monte Carlo simulation package used for this work was the Photon History Generator (*14,15*), which models the emission, scatter and attenuation of photons in a heterogeneous phantom, followed by the photons' subsequent collimation and detection.

Simulations were performed for a 23.6-mm-thick parallel-hole collimator using a 32.5-cm radius of rotation. The isotope modeled was ^{99m}Tc, collected with a symmetric 20% energy window centered around 140 KeV into a 256 × 256 matrix, resulting in counts of 600–700 kilocounts per view when no defects were present. The views collected were: anterior, posterior, both laterals, anterior obliques and posterior obliques.

Adhering to the terminology established in previous human studies (*6*), a "negative" image is one in which there is a defect with no activity, and the "positive" image shows activity in the area of the defect alone.

A series of 18 studies was performed, each of which contained a single defect involving 100% of a segment. In each case, a negative image and a positive image were produced. The images were considered to be suitable for diagnostic purposes by all the clinical observers.

A method for determining the best view for a defect in each segment was implemented. Eighteen film images showing all eight views of each study were presented to four experienced nuclear medicine physicians. The observers were informed that there was only one defect present and were asked to rank the best three views in decreasing order of the information content that was provided for reporting purposes.

RESULTS

Figure 1 shows the anterior, posterior, lateral, and anterior and posterior oblique projections of a normal study using the Monte Carlo simulation technique and the corresponding views of the segmented CT lung phantom. Figure 2 is a guide to the segments shown in each view.

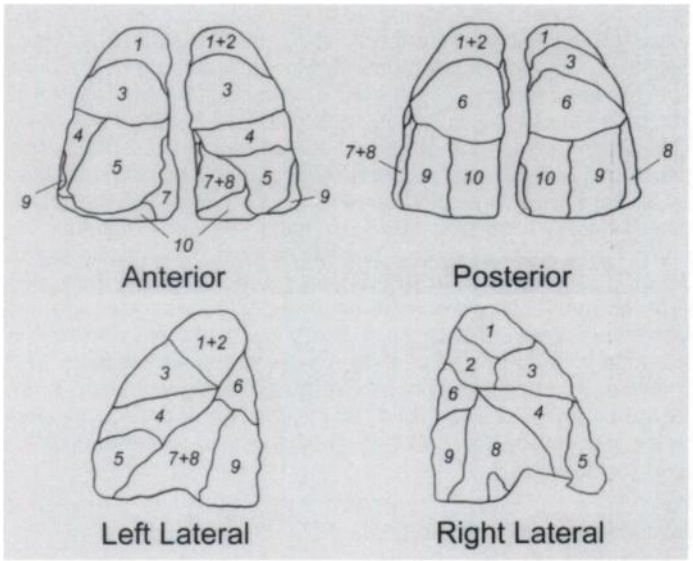

FIGURE 2. Four guide diagrams (anterior, posterior, left lateral and right lateral) of the segmented CT phantom are shown, with the segments labeled. (Right) Upper lobe: −1, apical; 2, posterior; 3, anterior. Middle lobe: −4, lateral; 5, medial. Lower lobe: −6, superior; 7, medial basal; 8, anterior basal; 9, lateral basal; 10, posterior basal. (Left) Upper lobe: 1+2, apicoposterior; 3, anterior. Lingular: 4, superior; 5, inferior. Lower lobe: 6, superior; 7+8, anteromedial basal; 9, lateral basal; 10, posterior basal.

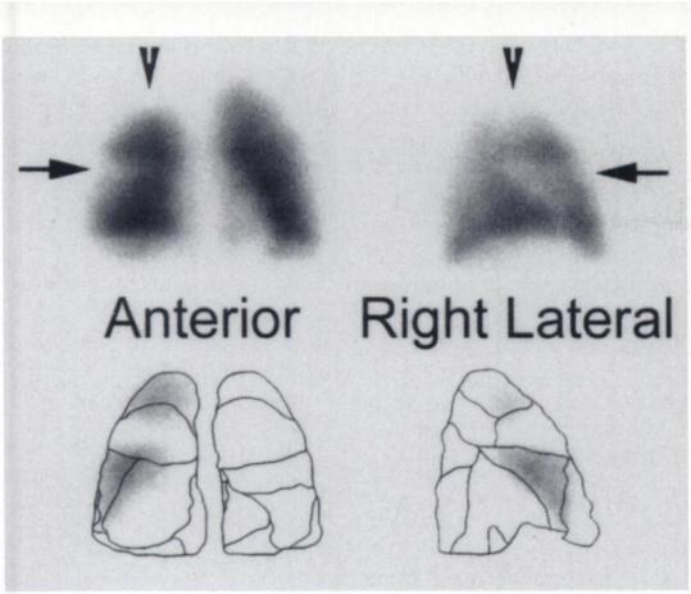

FIGURE 3. Defects in the right lung of the apical segment of the upper lobe (arrowheads) and the lateral segment of the middle lobe (arrows) are shown. The anterior and right lateral views are shown (upper). (Lower) The segmental outlines are superimposed on the positive images.

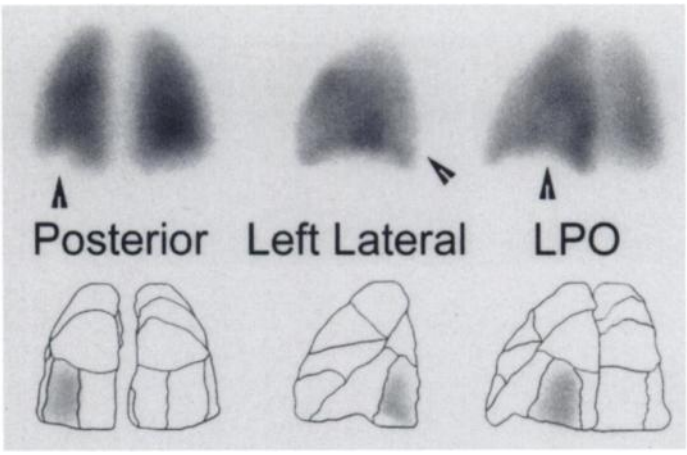

FIGURE 5. Defects in the left lung of the lateral basal segment are shown (arrowheads). The posterior, left lateral and left posterior oblique views are shown (upper). (Lower) The segmental outlines are superimposed on the positive images.

A selection of images from the simulations performed are shown in Figures 3–6. These figures show examples of both negative and positive images. For illustrative purposes, restricted views are shown in each case, and several of the figures demonstrate two segmental defects.

Table 1 shows the view that best demonstrates each segmental defect and up to two other acceptable views. The medial basal segment in the right lung was undetectable in any view.

Table 2 shows the frequency with which each view appears in the "best" column of Table 1. Segments are shown in two groups: all segments and those segments in the lower lobes. Because the medial basal segment in the right lower lobe was undetectable in any view, it was not included in the table.

DISCUSSION

The model of the lungs used in this study has the potential to provide answers to a multitude of questions regarding lung scintigraphy. A question as seminal as what views constitute a standard lung scan has not been satisfactorily resolved. This resolution has proved elusive in the conventional clinical setting due to the difficulty in defining the true segmental anatomy of the lungs. Scintigraphic segmental anatomy was admirably addressed in the work of Morrell et al. (*6*) in normal volunteers. This study was achieved by bronchoscopic cannulation of the segmental bronchi and ventilation of each segment with ^{81m}Kr to produce a positive image of the segment, with no contribution of activity from other lung tissue, and then occlusion of the same bronchus and ventilation of the remainder of the lungs were performed to produce a negative image of the segment. Many technical difficulties were encountered due to the inability to easily move the patients with the bronchoscope in situ, interference from local anesthetic instillations, limited views and radiation exposure to the volunteers. The model we used did not have these restrictions because eight standard views were obtained for every segment, defect size was precisely known, as were the contributions of scatter, and attenuation and

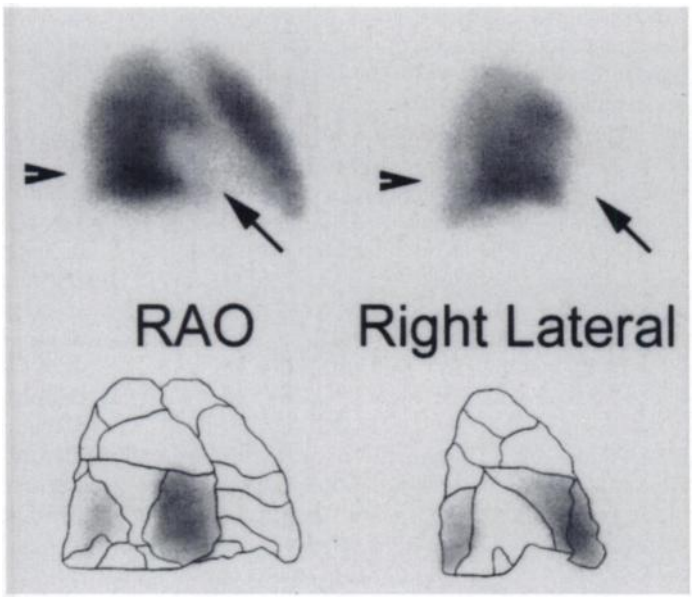

FIGURE 4. Defects in the right lung of the medial segment of the middle lobe (arrows) and the lateral segment of the lower lobe (arrowheads). The right anterior oblique and the right lateral views are shown (upper). (Lower) The segmental outlines are superimposed on the positive images.

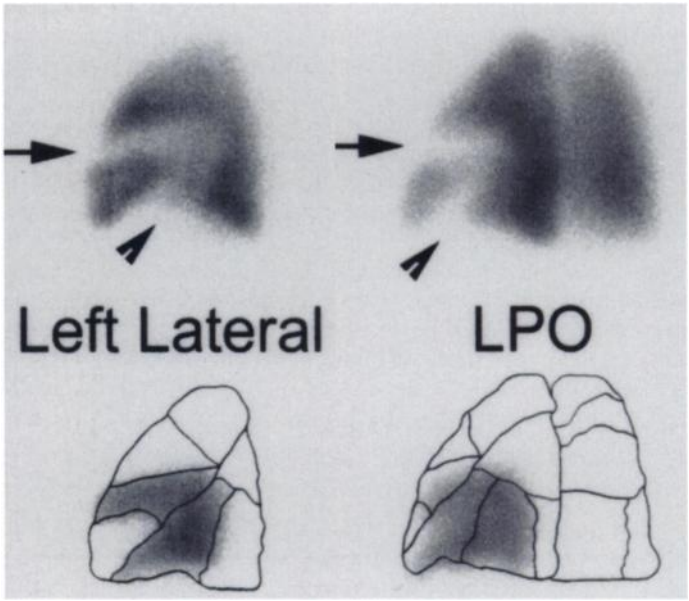

FIGURE 6. Defects in the left lung of the superior lingula (arrows) and the anteromedial basal segment of the lower lobe (arrowheads). The left lateral and the left posterior oblique views are shown (upper). (Lower) The segmental outlines are superimposed on the positive images.

TABLE 1
Best Views for Each Segment

Segment	Best	Acceptable	Acceptable
Right upper lobe			
Apical	Ant	RAO	Post
Posterior	RPO	R Lat	
Anterior	RAO	R Lat	
Right middle lobe			
Lateral	Ant	R Lat	RPO
Medial	RAO	Ant	R Lat
Right lower lobe			
Apical	RPO	R Lat	
Medial			
Anterior	RAO	RPO	
Lateral	RAO	RPO	Post
Posterior	RPO		
Left upper lobe			
Apicoposterior	L Lat	Post	LPO
Anterior	LAO	L Lat	
Lingula			
Superior	L Lat	LAO	Ant
Inferior	L Lat	LAO	
Left lower lobe			
Apical	LPO	L Lat	
Anteromedial	L Lat	LPO	
Lateral	Post		
Posterior	LPO	Post	

L Lat = left lateral; LAO = left anterior oblique; Ant = anterior; RAO = right anterior oblique; R Lat = right lateral; RPO = right posterior oblique; Post = posterior; LPO = left posterior oblique.

the images used in reporting were technically optimized for counts.

The veracity of the images in this virtual model is clearly dependent on an accurate knowledge of the segmental anatomy of the lungs. Three major sources were drawn upon in developing the model: lobar fissures apparent in CT scans of normal lungs; the best available anatomy illustrations from Netter (*11*) and Gray's Anatomy (*12*); and injection of color-coded material into the segmental bronchi of cadaveric lungs, followed by thin sectioning and digitization of the datasets (*8*). The virtual model provided a composite three-dimensional model of the segmental anatomy of the lungs that did not differ significantly from the planar illustrations found in the standard anatomy texts. Minor differences were present in the basal segments, but these were within the gamut of normal variation described in Boyden (*16*). Coding of this information was then transferred to the original CT phantom of the lungs used for the Monte Carlo simulations.

Four experienced nuclear medicine physicians viewed the data in a blinded fashion to determine the best views for each segment in eight standard views of the lungs. These data, as presented in Table 1, show some unexpected findings, particularly in the upper lobes of both lungs, where the anterior and RAO views were found to be the best for the right apical segment (Fig. 3) and where the lateral and posterior views were the best for the left apicoposterior segment. The unexpected findings may reflect removal of the problem of shoulder attenuation in the right lateral view and the more extensive posterior extension of the left apicoposterior segment, as compared with the relative anterior extension of the right apical segment.

TABLE 2
Frequency of Each Projection As the Best View

Projection	All segments	Only the lower lobes
Anterior	2	0
Posterior	1	1
Anterior obliques	5	2
Posterior obliques	5	4
Laterals	4	1

Other unexpected findings included the best visualization of the right middle lobe in the anterior and RAO projections rather than in the lateral view (Figs. 3 and 4), which is probably due to presentation of the greatest area of the middle lobe anteriorly and by the reduction of scatter from the medial border in the RAO due to the adjacent heart. This finding also may account for the unexpected number of segments that were best delineated in the RAO view of the right lung (4 of 10). Similarly, the best view of the lateral basal segment of the left lung was the posterior view (Fig. 5), suggesting that a combination of reduced scatter from the anteromedial and posterior segments and its peripheral localization in this view provided the best contrast. These contributions are more significant in degrading its delineation in the lateral view. Apart from this finding, four of nine segments in the left lung were best visualized in the left lateral projection (Fig. 6 and Table 2).

These results generally agree with those of Morrell et al. (*6*). In 9 of 18 segments, we had complete agreement about the best views. In 5 of 18 segments, we disagreed by one view due to the use of an anterior projection. In 2 of 18 segments, we disagreed by two views, also due to the use of an anterior projection. In the remaining two segments, we disagreed by one and two views, based on similar projections. We were in complete agreement about the failure to visualize a defect in the medial basal segment of the right lung in any view.

Practical application of the findings of this study have significance as multiheaded instruments become commonplace. Optimally, eight views can be obtained from four positions of a dual-headed instrument or further expedited by two positions of a triple-headed instrument, in which the index head is placed laterally, with the other two heads acquiring the anterior and posterior oblique projections. This compromise for speed and throughput forsakes the anterior and posterior views, with the loss of optimal imaging of three segments, only one of which is basal, and accepts the second-best views by using obliques for two of these. One segment, the lateral basal segment of the left lung, will not be clearly viewed in this instance.

The case for single-headed instruments is more complex. Clearly, the acquisition of eight standard views is too costly in terms of time and throughput. Which views to exclude then becomes an important question, one that has been grappled with since 1977 and has largely centered on the anterior oblique views. It raises the issue that several authors, including Morrell et al. (*6*) and Nielsen et al. (*17*), have raised: should the lateral replace the anterior oblique view or should the anterior oblique view be included at all? This is the first study to address these questions in terms of the eight standard views with well-defined and known segmental defects. Nielsen et al. (*17*) based their observations on 229 patients, of which 77 were classified as "normal" or minimally abnormal, based on clinical history and blood gases. They did not know the nature of the abnormalities that were reported as "abnormal" and classified these as diffuse or focal. Based on a simple qualitative reporting scale, it was concluded that the anterior oblique views did not contribute substantial information to the perfusion lung scan. Morrell et al. (*6*) chose to omit the anterior obliques based on this study.

The findings in our study certainly highlight that the anterior

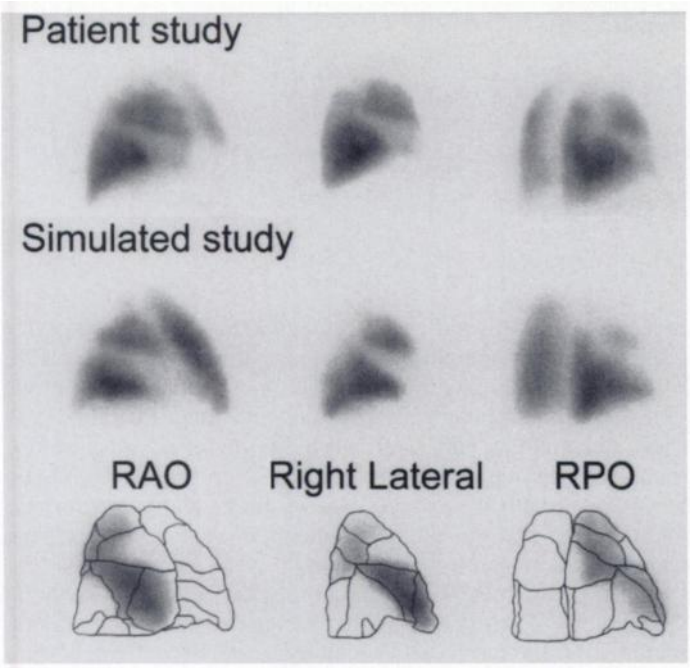

FIGURE 7. Simulation of the perfusion defects found in an actual study of a patient with a high probability of pulmonary embolic disease. The involved segments also are shown as "positive" images in the accompanying diagram of the segmental outlines.

oblique projection does contribute significant information. Figure 3 clearly shows its importance, particularly in the right lung, where it was found to contain information on more segments than the right posterior oblique and lateral projections. Its contribution in defining the segmental anatomy in the left lung is significantly less important than the left lateral and posterior oblique projection. A good case could be made for dropping the anterior and left anterior oblique projection from the eight standard views to expedite the scanning process without the loss of significant diagnostic data. The second-best views would provide the requisite information on the two segments involved (apical segment of the right upper lobe and anterior segment of the left upper lobe).

Such findings affirm the prevailing rule that a thorough knowledge of segmental anatomy is critical to the interpretation of lung scans. Although our model does not change the current concepts of planar segmental anatomy, it provides a three-dimensional scintigraphic atlas of this anatomy that could be powerful in unraveling segmental boundaries for tomographic imaging of the lungs. It allows the development of a well-controlled teaching tool with more accurate and reproducible abnormalities than previous "ad hoc" examples (Fig. 7). The Photon History Generator also allows the statistical determination of scatter fractions and a more workable and precise measure of attenuation. These issues will be explored in further work on the detectability of lesions based on size and the important contributions of scatter, attenuation and "shine-through" in scan interpretation.

CONCLUSION

An accurate virtual lung scan model of segmental anatomy has been produced with current technology overcoming the problems associated with a similar endeavor in vivo. The model was used to generate clearly defined and reproducible segmental abnormalities. This allowed the production of high-quality images in the eight standard views that permitted the determination of the best projections for viewing segmental anatomy in the clinical setting. A relatively high proportion of segmental data about the right lung is encoded in the right anterior oblique view and for the left lung in the left lateral view.

ACKNOWLEDGMENTS

This work was supported by research grants from the Nuclear Medicine Research Foundation, Department of Nuclear Medicine, Concord Hospital, Concord, Australia.

REFERENCES

1. Gottschalk A, Juni JE, Sostman HD, et al. Ventilation-perfusion scintigraphy in the PIOPED study. Part I. Data collection and tabulation. *J Nucl Med* 1993;34:1109–1118.
2. Gottschalk A, Sostman HD, Coleman RE, et al. Ventilation-perfusion scintigraphy in the PIOPED study. Part II. Evaluation of the scintigraphic criteria and interpretations. *J Nucl Med* 1993;34:1119–1126.
3. Carbonell AM, Landis GA, Miale A, Moser KM. Construction and testing of a thorax-lung phantom to aid in scintiphotograph interpretation. *Invest Radiol* 1969;4: 275–285.
4. Mandell CH. *Scintillation camera lung imaging: an anatomic atlas and guide.* London: Grune and Stratton; 1976.
5. Poulose K, Reba RC, Wagner HN. Characterization of the shape and location of perfusion defects in certain pulmonary diseases. *N Engl J Med* 1968;279:1020–1025.
6. Morrell NW, Roberts CM, Jones BE, Nijran KS, Biggs T, Seed WA. The anatomy of radioisotope lung scanning. *J Nucl Med* 1992;33:676–683.
7. Fogelman I, Maisey MN, Clarke SE. *An atlas of clinical nuclear medicine*, 2nd Ed. London: Martin Dunitz; 1994:523–526.
8. Magnussen J, Chicco P, Vu D, et al. Study of sectional segmental anatomy of the human lung using gelatin embedded sections and CT imaging techniques [Abstract]. In: *Proceedings of the 1996 conference of the anatomical society of Australia and New Zealand (10–12 July 1996).* Sydney: Anatomical Society of Australia and New Zealand; 1996:22.
9. Zubal IG, Harrell CR, Smith EO, Rattner Z, Gindi G, Hoffer PB. Computerized three-dimensional segmented human anatomy. *Med Phys* 1994;21:299–302.
10. NM/MIRD. *Estimates of specific absorbed fractions for photon sources uniformly distributed in various organs of a heterogeneous phantom.* New York: Society of Nuclear Medicine Publication; 1978:5.
11. Netter FH Colacino S, eds. *Atlas of human anatomy.* Basel: Ciba-Geigy; 1989:188–189.
12. Gray H, Williams PL, Warwick R, Dyson M, et al., eds. *Gray's anatomy*, 37th Ed. Edinburgh: Churchill Livingstone; 1989;1130p.
13. Agur AMR, Lee MJ, Gardner JN, eds. *Grant's atlas of anatomy*, 9th Ed. Baltimore: Williams and Wilkins; 1991:36–37.
14. Lewellen TK, Anson CP, Haynor DR, et al. Design of a simulation system for emission tomographs [Abstract]. *J Nucl Med* 1988;29:871.
15. Haynor DR, Harrison RL, Lewellen TK. The use of importance sampling techniques to improve the efficiency of photon tracking in emission tomography simulations. *Med Phys* 1991;18:990–1001.
16. Boyden EA. *Segmental anatomy of the lungs: a study of the patterns of the segmental bronchi and related pulmonary vessels.* New York: McGraw-Hill; 1955.
17. Nielsen PE, Kirchner PT, Gerber FH. Oblique views in lung perfusion scanning: clinical utility and limitations. *J Nucl Med* 1977;18:967–973.